

Synergy of Binary Substitutions for Improving the Cycle Performance in LiNiO₂ Revealed by Ab Initio Materials Informatics

Tomohiro Yoshida¹, Ryo Maezono^{2,3}, and Kenta Hongo^{4,3,5,6}

¹ *Department of Computer-Aided Engineering and Development,*

Sumitomo Metal Mining Co., Ltd., 3-5, Sobiraki-cho, Niihama, Ehime 792-0001, Japan

² *School of Information Science, JAIST, Asahidai 1-1, Nomi, Ishikawa, 923-1292, Japan*

³ *Computational Engineering Applications Unit, RIKEN,*

2-1 Hirosawa, Wako, Saitama 351-0198, Japan

⁴ *Research Center for Advanced Computing Infrastructure,*

JAIST, Asahidai 1-1, Nomi, Ishikawa 923-1292, Japan

⁵ *Center for Materials Research by Information Integration,*

Research and Services Division of Materials Data and Integrated System,

National Institute for Materials Science, 1-2-1 Sengen, Tsukuba, Ibaraki 305-0047, Japan and

⁶ *PRESTO, Japan Science and Technology Agency,*

4-1-8 Honcho, Kawaguchi-shi, Saitama 322-0012, Japan

(Dated: January 10, 2020)

We explore LiNiO₂-based cathode materials with two-element substitutions by an ab initio simulation based materials informatics (AIMI) approach. According to our previous study, a higher cycle performance strongly correlates with less structural change during charge–discharge cycles; the latter can be used for evaluating the former. However, if we target the full substitution space, full simulations are infeasible even for all binary combinations. To circumvent such an exhaustive search, we rely on Bayesian optimization. Actually, by searching only 4% of all the combinations, our AIMI approach discovered two promising combinations, Cr-Mg and Cr-Re, whereas each atom itself never improved the performance. We conclude that the synergy never emerges from a common strategy restricted to combinations of “good” elements that individually improve the performance. In addition, we propose a guideline for the binary substitutions by elucidating the mechanism of crystal structure change.

I. INTRODUCTION

Lithium-ion batteries (LIBs) have a high-voltage and high-capacity and hence are widely used as secondary batteries for mobile devices and hybrid/electric cars.^{1,2} The cathode material in LIBs is one of the most important factors that determine the battery performance. Thus, its development has recently attracted much attention from the viewpoint of industrial applications. A practical solution for improving the performance is “atomic substitution.”^{3–18} For example, consider LiNiO₂ (LNO)^{19–21}, which is known to have a higher capacity and lower cost than LiCoO₂ (LCO). However, LNO has fewer cycle characteristics than LCO. Indeed, the substitution of Ni sites in LNO with Co and Al, Li(NiCoAl)₂, – a commercially used cathode material – has prolonged the cycle life compared to LNO itself. Note that Co and Al are respectively known to improve the rate performance and thermal stability.^{22–25} This indicates that “individually good” elements come together to tune the corresponding characteristics. This is a commonly used strategy for improving battery performances. A situation may occur, however, where a combination of “no-good” elements has the potential of improving the performance. But it is really unclear if such a synergistic effect emerges. Unfortunately, however, we cannot straightforwardly establish an experimental verification even for binary substitutions having a huge number of possible combinations. This is because such an exhaustive search

based on experiments requires enormous amounts of time and high costs for the synthesis of candidate materials.

One of the most promising solutions to the above exhaustive search problem is materials informatics (MI)^{26–28} – a recently emerging paradigm in materials science combined with information and data science. There are a number of successful MI studies that have explored new materials with desirable properties.^{29–35} Since a sufficiently large amount of experimental data on material properties is generally unavailable unlike in other research areas (e.g., Bioinformatics), computational approaches are useful for generating the data. In most cases regarding electronic properties, ab initio simulations can satisfactorily generate data to construct machine learning-based prediction models, thereby tackling the exhaustive search problem. This may be called “ab initio Materials Informatics” (AIMI), though computationally proposed candidates should be verified experimentally. In battery materials, AIMI approaches have been used successfully to explore cathode coating materials³³, and new cathodes with a better capacity and thermal stability³⁴.

Focusing on the cycle performance of LIBs, an AIMI approach based on a high throughput screening combined with density functional theory (DFT) calculations has been applied to co-substituted LiFePO₄ cathode materials, and it successfully found element combinations that could prolong the cycle characteristics.³⁵ The volume change during the charge–discharge cycle and planer mismatch adopted in their study worked as the screen-

ing criterion. This success can be attributed to the fact that capacity fading is caused by microcracks during charge–discharge cycles³⁶, though ab initio simulations cannot directly evaluate the cycle performance. Very recently, we have investigated which unary substitutions improve the LNO cathode by computational screening.³⁷ Our findings are as follows: (i) DFT simulations must incorporate van der Waals (vdW) corrections in exchange–correlation functionals adopted in order to describe the structural changes during electrochemical cycling; (ii) c -axis contraction is more essential for the cycle characteristics; (iii) our descriptor analysis based on sparse modeling elucidates important descriptors correlating with the contraction. Finally, our AIMI approach indicated that Nb is the most promising candidate for the substitute element.

Our previous study provides the basis for the further exploration of new cathode materials beyond unary substitutions. As we mentioned before, however, binary substitutions have a much larger search space, so we employ a Bayesian optimization technique^{38,39} to efficiently discover the best binary combinations from the huge search space. In this study, we efficiently found synergetic binary substitutions by computing only about 4% of the search space, and we elucidate the mechanism of structural changes in a MI manner, which will be helpful for further explorations by AIMI approaches.

II. METHODOLOGY

All our ab initio DFT simulations were carried out by using the Vienna Ab initio Simulation Package (VASP)^{40,41} with the projector augmented wave (PAW) potentials. The plane-wave basis set cutoff energy and k -point mesh were set to be 650 eV and $3 \times 3 \times 1$, respectively, throughout this study. We employ the van der Waals exchange–correlation (vdW-XC) functional^{42,43} to accurately describe the crystal structural change during the charge–discharge cycle. Fig. 1 shows the LNO crystal structure with a rhombohedral $R\bar{3}m$ unit cell²¹. The super cell used in the study is $2 \times 2 \times 1$ of the conventional cell. We assume that doping elements are dissolved in the Ni sites. For unary substitutions, we replace Ni with X (Ni: X =92:8); for binary substitutions, each of the two Ni’s is replaced by X_1 and X_2 (Ni: X_1 : X_2 =84:8:8), respectively.

In order to design a high-capacity and high-cycle performance battery, we must limit the candidates. To extract approximately 80 % of Li with only Ni redox, the sum of valences of X_1 and X_2 must exceed 6. Upon the above limitation, the number of possible candidates amounts to 1,657 when considering the third and lower rows in the periodic table up to Pa (atomic number 91) except for the elements for which pseudo-potentials are unavailable. The structural changes are evaluated by the change in the crystal structures between 0 % and 83 % charged states. Although there are several possi-

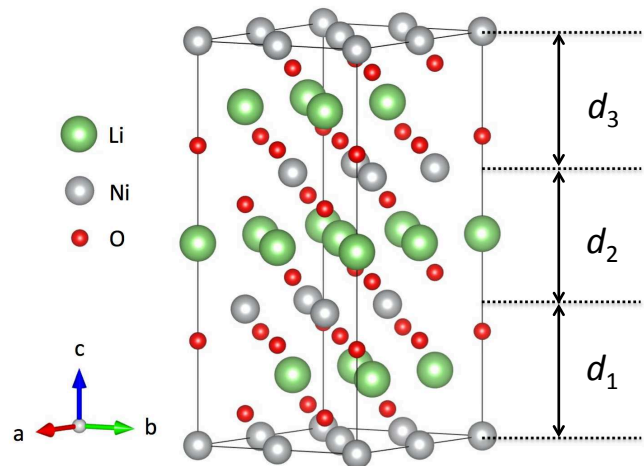


FIG. 1. Crystal structure of LiNiO₂. The super cell consists of four conventional cells. The structural change is measured as the average over interlayer distances, $d_{i=1-3}$ (see Text).

bilities for doping positions and a delithiated structure for each substitution, only the most stable structure is chosen by comparing their energies. According to our previous study³⁷, the cycle performance strongly correlates with the c -axis contraction, which is measured by the following quantity:

$$\Delta d_{\text{ave}} = \sum_{i=1}^3 \frac{|d_i^c - d_i^d|}{3} \quad (1)$$

where d_i^d (d_i^c) denotes interlayer distances for the discharged (charged) state (see Fig. 1).

We performed ab initio DFT simulations for all of the unary substitutions (65 elements) to evaluate Δd_{ave} . In the binary substitutions, all of the possible candidates amounted to $\sim 10^5$, but in reality such a huge number of simulations is infeasible. To efficiently discover the best binary combination(s), we thus adopted Bayesian optimization, which is an experimental design algorithm associated with Gaussian process regression.^{38,39} It has been reported that the design and choice of descriptors appropriate for describing material features uniquely are crucial for conducting Bayesian optimization.²⁹ The interlayer distances, d_i ($i = 1, 2, 3$), are determined as a balance between the ‘Coulomb repulsive interaction between oxygen in the NiO₆ layer’ and ‘vdW attractive interactions between the NiO₆’ layers^{44–49}. Although those interactions would be good descriptors, it is quite hard to directly evaluate them. Instead, as listed in Table I, we collected ‘elemental information of dopants’ and ‘structural information of 0 % charged state’ as descriptor candidates; all of the quantities were symmetrized with respect to the exchange between two dopants, *e.g.*, $m_{X_1} + m_{X_2}$ and $m_{X_1} \times m_{X_2}$ for atomic mass m ; we eventually selected those quantities as descriptors by random sampling. Based on Gaussian regression with the

descriptors selected above, we constructed a prediction model of Δd_{ave} and then performed Bayesian optimization under the maximum probability of improvement (as an acquisition function). We employed the Common Bayesian Optimization Library (COMBO)⁵⁰ to implement our Bayesian optimization.

III. RESULTS AND DISCUSSION

Δd_{ave} values for all of the unary substitutions (65 elements) are summarized in the Appendix. Their comparisons with LNO value ($\Delta d_{\text{ave}} = 0.156 \text{ \AA}$) classify the binary substitutions into ‘positive element’ and ‘negative element’ substitutions depending on whether or not it suppresses a structural change, *i.e.*, the positive/negative has a Δd_{ave} value less/greater than 0.156 \AA . Furthermore, the negative elements can be divided into the following two groups: the ones that dissolved into the Ni site and the others that moved from the Ni site to the Li site by structural relaxation.

V is the best dopant among the unary substitutions, having $\Delta d_{\text{ave}} = 0.124 \text{ \AA}$. We note that Zr and Na are classified into negative elements by the ab initio simulations, but these elements are known to improve cycle performance as follows: Zr stabilizes the cation ordering of Li and Ni¹⁶; Na stabilizes solid solutions at the Li site (pillar effect)¹⁸. These effects are beyond the scope of the present simulations, so we no longer consider these elements, which prevents us from obtaining inconsistent results.

As mentioned above, V is the best element for the unary substitutions. Here, we investigate if binary substitutions further suppress Δd_{ave} by using Bayesian optimization.^{38,39} First, we randomly select 31 candidates and evaluate their Δd_{ave} values by ab initio DFT simulations. Next, by using the descriptors shown in Table I, we construct a prediction model of Δd_{ave} based on the Gaussian process regression learned from the data set. We finally conduct Bayesian optimization for exploring the best binary combinations.

Figure 2 shows how quickly the Bayesian optimization and random search found the smallest Δd_{ave} . For Bayesian optimization, we considered two sets of descriptors including all and the ‘best’ selected ones (explained later). The average number of observations (N_{ave}) required for finding the optimized solution using Bayesian optimization with all of the descriptors and the random search were 13 and 15, respectively. As can be seen in Fig. 2, the Bayesian optimization rapidly reaches the smallest Δd_{ave} as compared with the random search, but its efficiency is not so high. In particular, when the number of observations is less than 15, the success probability of Bayesian optimization with a set of all of the descriptors is comparable to that of random sampling. This is probably because the set of all of the descriptors shown in Table I is inefficient for predicting Δd_{ave} accurately. Therefore, as explained below, we conducted the descrip-

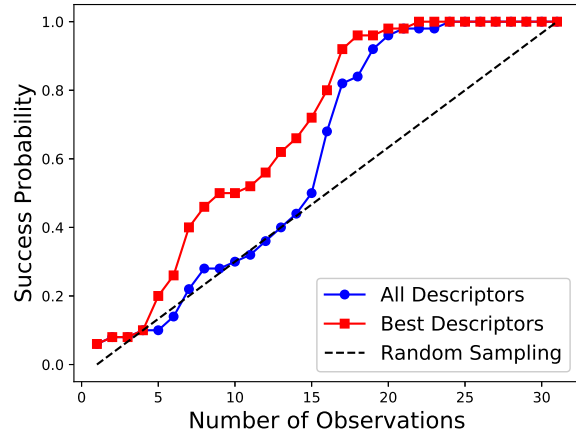


FIG. 2. Success probability for the Bayesian optimization with all of the descriptors (blue) and the best descriptors (red). Random sampling (black) is also shown for comparison.

tor analysis by LASSO regression⁵¹ and then extracted the most important ones in terms of the Δd_{ve} prediction; we anticipate this reduced set of descriptors can improve the efficiency of Bayesian optimization.

In our descriptor analysis, we first divide the data into training/test sets with the ratio of 8/2. The prediction model of Δd_{ave} is based on the LASSO regression learned from the training set. With the use of this trained model, we predict Δd_{ave} values for the test set and compare them to the corresponding ab initio values. Its prediction accuracy is evaluated in terms of the mean square error. The LASSO is known to automatically select important descriptors for prediction. As a result, we obtained six descriptors (V , α , $m_{X1} \times m_{X2}$, $EN_{X1} \times EN_{X2}$, a , $z_{X1} \times z_{X2}$), and by using them, Bayesian optimization was implemented again, which is denoted by the ‘best descriptors’. As expected, N_{ave} was 10 for the best descriptors, and the success probability improved (see Fig. 2). We thus expect that these descriptors are efficient even with further searches, and then, we proceed with the Bayesian optimization for the remaining 1,626 candidates.

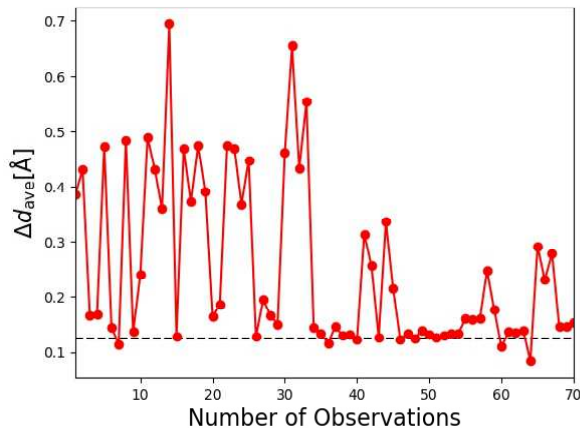
Thirty nine times observations for the Bayesian optimization with the best descriptors were carried out after 31 times observations for random sampling, where their search history is shown in Figure 3. Meanwhile, the random sampling (observation #: 1~31) chooses Δd_{ave} values distributed from large to small values, and the Bayesian optimization (32~70) selects smaller Δd_{ave} values (N.B., our acquisition function is the maximum probability of improvement as described in the Methodology section).

From the above observations by the Bayesian optimization, we discovered V-Ga, Ti-Fe, Al-Mn, Al-Cr, Mg-Cr, and Cr-Re as the combinations that suppress Δd_{ave} better than the best unary substitution. Although V-Ga

elemental information	crystal structure information
atomic number Z	lattice volume V
atomic mass m	lattice constant a, b, c
electronegativity EN	angle formed by basic vector α, β, γ
covalent radius CR	substituted positions of X_1 and X_2 x, y, z
first-ionization energy IE	
maximum oxidation state O	
coefficient of van der Waals C_6	

TABLE I. List of descriptors considered in the present study.

positive element	negative element
V,Nb,Ge,Ir,Au	Pb,Pa,Hf,Rh,Fe,Cu
Al,Ti,Ta,Mg,Ga	Po,W,Zn,Cr,Zr,Pd
Ru,Bi,Dy,Os,Sb	Mo,Ca,Yb,Cd,Ag
Mn,Tc,Y,Tb,Re	Gd*,Ce*,Eu*,Tl*,Pm*,Sm*
Tm,Lu,Pt,Ho,In	Hg*,Na*,Th*,Nd*,Pr*,Sr*
Er,Sc,Sn	La*,Ac*,Ba*,Ra*,K*,Rb*
	Fr*,Cs*

TABLE II. Classification of presence/absence of the Δd_{ave} suppression effect in unary substitutions. In the negative element, the element marked with * moves from the Ni site to the Li site.FIG. 3. Search history for the binary substitutions. Black-dashed line shows the smallest Δd_{ave} for the unary substitutions.

and Al-Mn are composed of positive elements, the other combinations include negative elements, Fe or Cr. Nevertheless, for the latter, their Δd_{ave} values showed more suppression as compared to the best unary substitution, which can be interpreted as being synergistic effects.

In order to elucidate why the synergy emerges, the suppression mechanism in the binary substitutions is investigated here. We construct a regression model of Δd_{ave} predictions learned from 27 combinations where dopants

do not move to the Li sites. Changes in interlayer distances d during cycling are anticipated to be determined by the “Coulomb repulsive interaction between oxygen in the NiO₆ layer,” “vdW attractive interactions between the NiO₆ layers,” “ionic radii of doping cations,” etc. Accordingly, the following quantities are considered as our descriptors entering the regression model: “a product of the averaged Bader charges^{52,53} over the facing oxygen layers,” “a sum of the averaged vdW coefficients over the facing Ni-O slabs,” “a sum of the averaged ionic radii over the facing Ni layers,” and “the difference in the averaged Bader charges within the oxygen layer between charged and discharged states.” In total, we obtained 10 descriptors for the Δd_{ave} prediction. At the charge rate used in this study, Ni-O slabs can be classified into the following two cases [see Fig. 4 (a)]: (A) Ni-O slabs sandwiching a Li-discharged layer and (B) Ni-O slabs sandwiching a Li-charged layer. The above descriptors are calculated for each case. Note that two independent O layers exist in the (B) Ni-O slab and the corresponding descriptors distinguished by their magnitudes are independently treated.

We consider all possible combinations of 10 descriptors to construct the regression models. Figure 4 (b) shows their regression coefficients in a heat map form. Looking at models with higher R^2 (coefficient of determination) values, it can be seen that the charged product of the oxygen layer (A)/the sum of the vdW coefficient has a negative/positive contribution. This is because the larger Coulomb repulsion and smaller vdW attraction suppress a shrinkage in the c -axis direction. These two descriptors are the most important factors describing the change along the c -axis. In other words, in order to improve the cycle characteristics, it is preferable to substitute Ni atoms with those which have a low vdW coefficient, holding large Bader charges on oxygen layers. We also found that a large change in the Bader charge on oxygen accompanying the charge-discharge cycle significantly contributes to the suppression of structural change. This is because a smaller change in the electronic structure during the charge/discharge cycle suppresses the structural change. Although the ionic radius of the cation is less important than the product of the oxygen charge and sum of the vdW coefficient, it is required for constructing an accurate model.

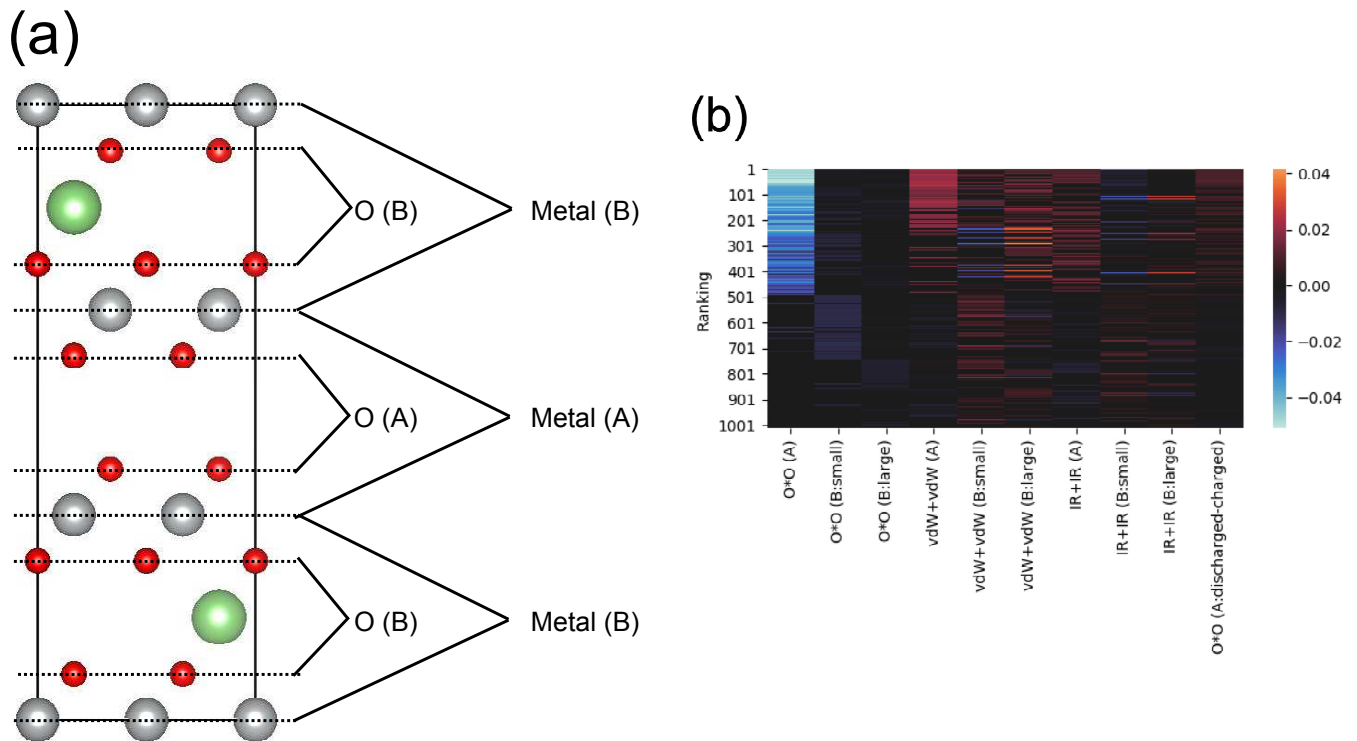


FIG. 4. (a) Descriptor classification. (A) Ni-O slabs sandwiching a Li-discharged layer and (B) Ni-O slabs sandwiching a Li-charged layer. (b) Heat map of regression coefficients arranged according to the models’ coefficient of determination R^2 . The largest R^2 was 0.77. From left, “a product of Bader charge on oxygen (A, B small, B large),” “a sum of vdW coefficients in the Ni-O slab (A, B small, B large),” “a sum of ionic radii of cations (A, B small, B large),” and “a difference in Bader charge on oxygen between charged and discharge states.” See Text for more details.

It should be noted that cations substituted with Ni require a small ionic radius in (A) and inversely a large one in (B). Consequently, any unary substitution cannot satisfy both the requirements simultaneously, and hence, its Δd_{ave} suppression is smaller than that of the binary substitution. In other words, these inverse requirements are the origin of the synergistic effects. Indeed, Cr-Re ($\Delta d_{\text{ave}} = 0.08\text{\AA}$) shows the most suppression of Δd_{ave} change, where a large Cr cation and a small Re cation are doped into (B) and (A), respectively. It is concluded that the understanding of why synergistic effects occur is important in order to design the best performance material.

IV. CONCLUSIONS

We investigated unary and binary substitutions in LiNiO_2 to improve its cycle performance. Owing to their strong correlation, the cycle characteristics were evaluated from the perspective of structural change along the c -axis during cycling, and this was investigated for various doping elements by using ab initio simulations. For the unary substitutions, an exhaustive search based on

the ab initio simulations revealed that V is the best for a unary substitution. As for the binary substitutions, our Bayesian optimization explored the candidate combinations more efficiently than random sampling, and results revealed synergistic effects for combinations of doping elements that never improved the cycle performance individually (Cr-Mg and Cr-Re). We also proposed guidelines for battery material design. Our ab initio materials informatics approach presented here can be regarded as a promising fundamental technique for further exploration of high-performance battery materials.

V. ACKNOWLEDGMENTS

The computations in this work were performed by using the facilities of RCACI (Research Center for Advanced Computing Infrastructure) at JAIST. T. Y. would like to thank T. Kosasa, K. Ryoshi, T. Toma, and S. Yoshio for their fruitful discussions and technical support. K. H. is grateful for financial support from KAKENHI grants (17K17762 and 19K05029), a Grant-in-Aid for Scientific Research on Innovative Areas (16H06439 and 19H05169), the FLAG-SHIP2020

project (MEXT for the computational resources, projects hp180206 and hp180175 at K-computer), and PRESTO (JPMJPR16NA) and the Materials research by Information Integration Initiative (MI²I) project of the Support Program for Starting Up Innovation Hub from the Japan Science and Technology Agency (JST). R. M. is grateful for financial support from MEXT-KAKENHI (project JP16KK0097), the FLAG-SHIP2020 project (MEXT for the computational resources, projects hp180206 and hp180175 at K-computer), and the Air Force Office

of Scientific Research (AFOSR-AOARD/FA2386-17-1-4049).

VI. APPENDIX

We summarize the calculated Δd_{ave} for unary substitution in Table III.

-
- ¹ Kang, K.; Meng, Y. S.; Bréger, J.; Grey, C. P.; Ceder, G. Electrodes with High Power and High Capacity for Rechargeable Lithium Batteries. *Science* **2006**, *311*, 977–980.
 - ² Manthiram, A.; Vadivel Murugan, A.; Sarkar, A.; Muraliganth, T. Nanostructured Electrode Materials for Electrochemical Energy Storage and Conversion. *Energy Environ. Sci.* **2008**, *1*, 621–638.
 - ³ Guilnard, M.; Rougier, A.; Grüne, M.; Croguennec, L.; Delmas, C. Effects of Aluminum on the Structural and Electrochemical Properties of LiNiO₂. *J. Power Sources* **2003**, *115*, 305–314.
 - ⁴ Guilnard, M.; Croguennec, L.; Denux, D.; Delmas, C. Thermal Stability of Lithium Nickel Oxide Derivatives. Part I: Li_xNi_{1.02}O₂ and Li_xNi_{0.89}Al_{0.16}O₂ (x = 0.50 and 0.30). *Chem. Mater.* **2003**, *15*, 4476–4483.
 - ⁵ Pouillier, C.; Croguennec, L.; Biensan, P.; Willmann, P.; Delmas, C. Synthesis and Characterization of New LiNi_{1-y}Mg_yO₂ Positive Electrode Materials for Lithium-Ion Batteries. *J. Electrochem. Soc.* **2000**, *147*, 2061–2069.
 - ⁶ Sathiyamoorthi, R.; Shakkthivel, P.; Ramalakshmi, S.; Shul, Y.-G. Influence of Mg Doping on the Performance of LiNiO₂ Matrix Ceramic Nanoparticles in High-Voltage Lithium-Ion Cells. *J. Power Sources* **2007**, *171*, 922–927.
 - ⁷ Kondo, H.; Takeuchi, Y.; Sasaki, T.; Kawachi, S.; Itou, Y.; Hiruta, O.; Okuda, C.; Yonemura, M.; Kamiyama, T.; Ukyo, Y. Effects of Mg-Substitution in Li(Ni,Co,Al)O₂ Positive Electrode Materials on the Crystal Structure and Battery Performance. *J. Power Sources* **2007**, *174*, 1131–1136.
 - ⁸ Cho, J.; Jung, H.; Park, Y.; Kim, G.; Lim, H. S. Electrochemical Properties and Thermal Stability of Li_aNi_{1-x}Co_xO₂ Cathode Materials. *J. Electrochem. Soc.* **2000**, *147*, 15–20.
 - ⁹ Delmas, C.; Saadoune, I.; Rougier, A. The Cycling Properties of the Li_xNi_{1-y}Co_yO₂ Electrode. *J. Power Sources* **1993**, *44*, 595–602.
 - ¹⁰ Saadoune, I.; Delmas, C. LiNi_{1-y}Co_yO₂ Positive Electrode Materials: Relationships Between the Structure, Physical Properties and Electrochemical Behaviour. *J. Mater. Chem.* **1996**, *6*, 193–199.
 - ¹¹ Rossen, E.; Jones, C.; Dahn, J. Structure and Electrochemistry of Li_xMn_yNi_{1-y}O₂. *Solid State Ionics* **1992**, *57*, 311–318.
 - ¹² Venkatraman, S.; Manthiram, A. Structural and Chemical Characterization of Layered Li_{1-x}Ni_{1-y}Mn_yO_{2-δ} (y = 0.25 and 0.5, and 0 ≤ (1-x) ≤ 1) Oxides. *Chem. Mater.* **2003**, *15*, 5003–5009.
 - ¹³ Mohan, P.; Kalaignan, G. P. Electrochemical Performance of Yttrium Substituted LiY_xNi_{1-x}O₂ (0.00 ≤ x ≤ 0.20) Cathode Materials for Rechargeable Lithium-Ion Batteries. *J. Nanosci. Nanotechnol.* **2014**, *14*, 5278–5282.
 - ¹⁴ Kwon, S. N.; Song, M. Y.; Park, H. R. Electrochemical Properties of LiNiO₂ Substituted by Al or Ti for Ni via the Combustion Method. *Ceram. Int.* **2014**, *40*, 14141–14147.
 - ¹⁵ Kim, H.-S.; Ko, T.-K.; Na, B.-K.; Cho, W. I.; Chao, B. W. Electrochemical Properties of LiM_xCo_{1-x}O₂ [M = Mg, Zr] Prepared by Sol-Gel Process. *J. Power Sources* **2004**, *138*, 232–239.
 - ¹⁶ Yoon, C. S.; Choi, M.-J.; Jun, D.-W.; Zhang, Q.; Kagazchi, P.; Kim, K.-H.; Sun, Y.-K. Cation Ordering of Zr-Doped LiNiO₂ Cathode for Lithium-Ion Batteries. *Chem. Mater.* **2018**, *30*, 1808–1814.
 - ¹⁷ Yoon, C. S.; Kim, U.-H.; Park, G.-T.; Kim, S. J.; Kim, K.-H.; Kim, J.; Sun, Y.-K. Self-Passivation of a LiNiO₂ Cathode for a Lithium-Ion Battery through Zr Doping. *ACS Energy Lett.* **2018**, *3*, 1634–1639.
 - ¹⁸ Kim, H.; Choi, A.; Doo, S. W.; Lim, J.; Kim, Y.; Lee, K. T. Role of Na⁺ in the Cation Disorder of [Li_{1-x}Na_x]NiO₂ as a Cathode for Lithium-Ion Batteries. *J. Electrochem. Soc.* **2018**, *165*, A201–A205.
 - ¹⁹ Myung, S.-T.; Maglia, F.; Park, K.-J.; Yoon, C. S.; Lamp, P.; Kim, S.-J.; Sun, Y.-K. Nickel-Rich Layered Cathode Materials for Automotive Lithium-Ion Batteries: Achievements and Perspectives. *ACS Energy Lett.* **2017**, *2*, 196–223.
 - ²⁰ Dahn, J.; von Sacken, U.; Michal, C. Structure and Electrochemistry of Li_{1±y}NiO₂ and a New Li₂NiO₂ Phase with the Ni(OH)₂ Structure. *Solid State Ionics* **1990**, *44*, 87–97.
 - ²¹ Ohzuku, T.; Ueda, A.; Nakayama, M. Electrochemistry and Structural Chemistry of LiNiO₂ (R $\bar{3}m$) for 4 V Secondary Lithium Cells. *J. Electrochem. Soc.* **1993**, *140*, 1862–1870.
 - ²² Ohzuku, T.; Ueda, A.; Nagayama, M.; Iwakoshi, Y.; Komori, H. Comparative Study of LiCoO₂, LiNi_{1/2}Co_{1/2}O₂ and LiNiO₂ for 4 Volt Secondary Lithium Cells. *Electrochim. Acta* **1993**, *38*, 1159–1167.
 - ²³ Ohzuku, T.; Ueda, A.; Kouguchi, M. Synthesis and Characterization of LiAl_{1/4}Ni_{3/4}O₂ (R $\bar{3}m$) for Lithium-Ion (Shuttlecock) Batteries. *J. Electrochem. Soc.* **1995**, *142*, 4033–4039.
 - ²⁴ Lee, K.; Yoon, W.; Kim, K.; Lee, K.; Hong, S. Characterization of LiNi_{0.85}Co_{0.10}M_{0.05}O₂ (M = Al, Fe) as a Cathode Material for Lithium Secondary Batteries. *J. Power Sources* **2001**, *97-98*, 308–312.

Element	$\Delta d_{\text{ave}}(\text{\AA})$	Element	$\Delta d_{\text{ave}}(\text{\AA})$	Element	$\Delta d_{\text{ave}}(\text{\AA})$
V	0.124	Pt	0.147	Ag	0.199
Nb	0.125	Ho	0.148	Gd	0.216
Ge	0.132	In	0.149	Ce	0.257
Ir	0.134	Er	0.149	Eu	0.283
Au	0.134	Sc	0.150	Tl	0.290
Al	0.135	Sn	0.155	Pm	0.306
Ti	0.135	Pb	0.159	Sm	0.314
Ta	0.135	Pa	0.160	Hg	0.337
Mg	0.135	Hf	0.160	Na	0.347
Ga	0.137	Rh	0.161	Th	0.385
Ru	0.137	Fe	0.161	Nd	0.395
Bi	0.139	Cu	0.162	Pr	0.420
Dy	0.139	Po	0.163	Sr	0.426
Os	0.140	W	0.165	La	0.440
Sb	0.140	Zn	0.167	Ac	0.493
Mn	0.141	Cr	0.167	Ba	0.574
Tc	0.141	Zr	0.169	Ra	0.622
Y	0.142	Pd	0.172	K	0.685
Tb	0.143	Mo	0.177	Rb	0.777
Re	0.144	Ca	0.189	Fr	0.856
Tm	0.146	Yb	0.191	Cs	0.865
Lu	0.147	Cd	0.193		

TABLE III. Δd_{ave} for unary substitution.

- ²⁵ Schipper, F.; Erickson, E. M.; Erk, C.; Shin, J.-Y.; Chesneau, F. F.; Aurbach, D. Review-Recent Advances and Remaining Challenges for Lithium Ion Battery Cathodes: I. Nickel-Rich, $\text{LiNi}_x\text{Co}_y\text{Mn}_z\text{O}_2$. *J. Electrochem. Soc.* **2017**, *164*, A6220–A6228.
- ²⁶ Ramprasad, R.; Batra, R.; Pilania, G.; Mannodi-Kanakkithodi, A.; Kim, C. Machine Learning in Materials Informatics: Recent Applications and Prospects. *npj Comput. Mater.* **2017**, *3*, 54.
- ²⁷ Agrawal, A.; Choudhary, A. Perspective: Materials Informatics and Big Data: Realization of the "Fourth Paradigm" of Science in Materials Science. *APL Mater.* **2016**, *4*, 053208.
- ²⁸ Potyrailo, R.; Rajan, K.; Stoewe, K.; Takeuchi, I.; Chisholm, B.; Lam, H. Combinatorial and High-Throughput Screening of Materials Libraries: Review of State of the Art. *ACS Comb. Sci.* **2011**, *13*, 579–633.
- ²⁹ Seko, A.; Togo, A.; Hayashi, H.; Tsuda, K.; Chaput, L.; Tanaka, I. Prediction of Low-Thermal-Conductivity Compounds with First-Principles Anharmonic Lattice-Dynamics Calculations and Bayesian Optimization. *Phys. Rev. Lett.* **2015**, *115*, 205901.
- ³⁰ Hautier, G.; Miglio, A.; Ceder, G.; Rignanese, G.-M.; Gonze, X. Identification and Design Principles of Low Hole Effective Mass p-Type Transparent Conducting Oxides. *Nat. Commun.* **2013**, *4*, 2292.
- ³¹ Ikebata, H.; Hongo, K.; Isomura, T.; Maezono, R.; Yoshida, R. Bayesian Molecular Design with a Chemical Language Model. *J. Computer-Aided Molecular Design* **2017**, *31*, 379–391.
- ³² Wu, S.; Kondo, Y.; Kakimoto, M.-a.; Yang, B.; Yamada, H.; Kuwajima, I.; Lambard, G.; Hongo, K.; Xu, Y.; Shiomi, J.; Schick, C.; Morikawa, J.; Yoshida, R. Machine-Learning-Assisted Discovery of Polymers with High Thermal Conductivity Using a Molecular Design Algorithm. *npj Comput. Mater.* **2019**, *5*, 66.
- ³³ Aykol, M.; Kim, S.; Hegde, V. I.; Snyder, D.; Lu, Z.; Hao, S.; Kirklin, S.; Morgan, D.; Wolverton, C. High-Throughput Computational Design of Cathode Coatings for Li-Ion Batteries. *Nat. Commun.* **2016**, *7*, 13779.
- ³⁴ Ceder, G. Opportunities and Challenges for First-Principles Materials Design and Applications to Li Battery Materials. *MRS Bull.* **2010**, *35*, 693–701.
- ³⁵ Nishijima, M.; Ootani, T.; Kamimura, Y.; Sueki, T.; Esaki, S.; Murai, S.; Fujita, K.; Tanaka, K.; Ohira, K.; Koyama, Y.; Tanaka, I. Accelerated Discovery of Cathode Materials with Prolonged Cycle Life for Lithium-Ion Battery. *Nat. Commun.* **2014**, *5*, 4553.
- ³⁶ Yoon, C. S.; Jun, D.-W.; Myung, S.-T.; Sun, Y.-K. Structural Stability of LiNiO_2 Cycled above 4.2 V. *ACS Energy Lett.* **2017**, *2*, 1150–1155.
- ³⁷ Yoshida, T.; Hongo, K.; Maezono, R. First-Principles Study of Structural Transitions in LiNiO_2 and High-Throughput Screening for Long Life Battery. *J. Phys. Chem. C* **2019**, *123*, 14126–14131.
- ³⁸ Jones, D. R.; Schonlau, M.; Welch, W. J. Efficient Global Optimization of Expensive Black-Box Functions. *J. Glob. Optim.* **1998**, *13*, 455–492.
- ³⁹ Shahriari, B.; Swersky, K.; Wang, Z.; Adams, R. P.; de Freitas, N. Taking the Human Out of the Loop: A Review of Bayesian Optimization. *Proc. IEEE* **2016**, *104*, 148–175.

- ⁴⁰ Kresse, G.; Furthmüller, J. Efficient Iterative Schemes for Ab Initio Total-Energy Calculations Using a Plane-Wave Basis Set. *Phys. Rev. B: Condens. Matter Mater. Phys.* **1996**, *54*, 11169–11186.
- ⁴¹ Kresse, G.; Furthmüller, J. Efficiency of Ab-Initio Total Energy Calculations for Metals and Semiconductors Using a Plane-Wave Basis Set. *Comput. Mater. Sci.* **1996**, *6*, 15–50.
- ⁴² Klimeš, J.; Bowler, D. R.; Michaelides, A. Van der Waals Density Functionals Applied to Solids. *Phys. Rev. B: Condens. Matter Mater. Phys.* **2011**, *83*, 195131.
- ⁴³ Klimeš, J.; Bowler, D. R.; Michaelides, A. Chemical Accuracy for the van der Waals Density Functional. *J. Phys.: Condens. Matter.* **2010**, *22*, 022201.
- ⁴⁴ Laubach, S.; Laubach, S.; Schmidt, P. C.; Enslin, D.; Schmid, S.; Jaegermann, W.; Thiβn, A.; Nikolowski, K.; Ehrenberg, H. Changes in the Crystal and Electronic Structure of LiCoO₂ and LiNiO₂ upon Li Intercalation and De-intercalation. *Phys. Chem. Chem. Phys.* **2009**, *11*, 3278–3289.
- ⁴⁵ Li, W.; Reimers, J.; Dahn, J. In Situ X-ray Diffraction and Electrochemical Studies of Li_{1-x}NiO₂. *Solid State Ion.* **1993**, *67*, 123–130.
- ⁴⁶ Pouillier, C.; Croguennec, L.; Delmas, C. The Li_xNi_{1-y}Mg_yO₂ ($y = 0.05, 0.10$) System: Structural Modifications Observed upon Cycling. *Solid State Ion.* **2000**, *132*, 15–29.
- ⁴⁷ Yabuuchi, N.; Makimura, Y.; Ohzuku, T. Solid-State Chemistry and Electrochemistry of LiCo_{1/3}Ni_{1/3}Mn_{1/3}O₂ for Advanced Lithium-Ion Batteries: III. Rechargeable Capacity and Cycleability. *J. Electrochem. Soc.* **2007**, *154*, A314–A321.
- ⁴⁸ chen Karen Chen-Wiegart, Y.; Liu, Z.; Faber, K. T.; Barnett, S. A.; Wang, J. 3D Analysis of a LiCoO₂-Li(Ni_{1/3}Mn_{1/3}Co_{1/3})O₂ Li-Ion Battery Positive Electrode Using X-Ray Nano-Tomography. *Electrochem. Commun.* **2013**, *28*, 127–130.
- ⁴⁹ Basch, A.; de Compo, L.; Albering, J. H.; White, J. W. Chemical Delithiation and Exfoliation of Li_xCoO₂. **2014**, *220*, 102–110.
- ⁵⁰ Ueno, T.; Rhone, T. D.; Hou, Z.; Mizoguchi, T.; Tsuda, K. COMBO: An efficient Bayesian optimization library for materials science. *Mater. Discov.* **2016**, *4*, 18–21.
- ⁵¹ R. Tibshirani, Regression Shrinkage and Selection via the Lasso. *J. R. Stat. Soc. Ser.* **1996**, *58*, 267–288.
- ⁵² Bader, R. F. W. *Atoms in Molecules: a Quantum Theory*; Oxford University Press: New York, 1990.
- ⁵³ Tang, W.; Sanville, E.; Henkelman, G. A Grid-Based Bader Analysis Algorithm without Lattice Bias. *J. Phys.: Condens. Matter* **2009**, *21*, 084204.